

# Low-Energy Direct Capture in the $^{16}\text{O}(\alpha,\gamma)^{20}\text{Ne}$ Reaction

P. Mohr\*

*Diakoniekrankenhaus Schwäbisch Hall, D-74523 Schwäbisch Hall, Germany*

(Dated: September 15, 2018)

The cross section of the  $^{16}\text{O}(\alpha,\gamma)^{20}\text{Ne}$  capture reaction is analyzed at low energies where the direct capture mechanism is dominant. For temperatures below  $T_9 = 0.2$  the resulting astrophysical reaction rate is about a factor of two higher than in a recent compilation whereas the energy dependence of the astrophysical S-factor and the branching ratios to the  $^{20}\text{Ne}$  bound states are very similar to previous calculations. The validity of the widely used detailed balance theorem for the inverse  $^{20}\text{Ne}(\gamma,\alpha)^{16}\text{O}$  photodisintegration rate is confirmed for the special case of high-lying first excited states.

PACS numbers: 25.55.-e, 21.60.Gx, 26.20.+f

## I. INTRODUCTION

The astrophysical reaction rate of the  $^{16}\text{O}(\alpha,\gamma)^{20}\text{Ne}$  reaction is dominated by a series of resonances in a broad range of high temperatures above  $0.2 \times 10^9 \text{ K}$  ( $T_9 \geq 0.2$ ). However, at low temperatures ( $T_9 < 0.2$ ) the direct capture mechanism becomes dominant [1].

The  $^{16}\text{O}(\alpha,\gamma)^{20}\text{Ne}$  reaction is an important reaction during helium burning in stars at typical temperatures around  $T_9 = 0.2$  which is the temperature range where both direct capture and resonances are important. The  $^{16}\text{O}(\alpha,\gamma)^{20}\text{Ne}$  reaction blocks the reaction chain  $3\alpha \rightarrow ^{12}\text{C}(\alpha,\gamma)^{16}\text{O}(\alpha,\gamma)^{20}\text{Ne}$  because there are no resonances in the so-called Gamow window which is located at  $E_0 \approx 1.22 (Z_1^2 Z_2^2 A_{\text{red}} T_6^2)^{1/3} \text{ keV}$  with a width of  $\Delta = 0.749 (Z_1^2 Z_2^2 A_{\text{red}} T_6^5)^{1/6} \text{ keV}$ ;  $Z_1$  ( $A_1$ ) and  $Z_2$  ( $A_2$ ) are the charge (mass) numbers of projectile and target, and  $A_{\text{red}} = A_1 A_2 / (A_1 + A_2)$  is the reduced mass number. At  $T_9 = 0.2$  one finds  $E_0 = 390 \text{ keV}$  and  $\Delta = 190 \text{ keV}$ . In several previous papers the S-factor at  $E_0 = 300 \text{ keV}$  is reported. The  $2^-$  state at  $E_x = 4967 \text{ keV}$  in  $^{20}\text{Ne}$  does not appear as resonance at  $E = 237 \text{ keV}$  in the  $^{16}\text{O}(\alpha,\gamma)^{20}\text{Ne}$  reaction because of its unnatural parity.

The inverse  $^{20}\text{Ne}(\gamma,\alpha)^{16}\text{O}$  reaction plays an important role in neon burning at significantly higher temperatures around  $T_9 = 1 - 2$  [2]. The reaction rate of photodisintegration reactions is usually derived from the capture rate using the detailed balance theorem (see e.g. [1]). The validity of this theorem for the case of the  $^{16}\text{O}(\alpha,\gamma)^{20}\text{Ne}$  and  $^{20}\text{Ne}(\gamma,\alpha)^{16}\text{O}$  reactions with high-lying first excited states is analyzed in the last section VI.

Direct capture in the  $^{16}\text{O}(\alpha,\gamma)^{20}\text{Ne}$  capture reaction has been analyzed theoretically by [3, 4, 5, 6, 7, 8]. Experimentally a non-resonant S-factor of  $S = 0.26 \pm 0.07 \text{ MeV b}$  for the ground state transition has been reported at energies around  $E = 2 \text{ MeV}$  [9], and a total S-factor of  $S(300 \text{ keV}) < 0.7 \text{ MeV b}$  was deduced, but this result has been questioned by [4]. Later, an upper limit of  $S < 3.37 \text{ MeV b}$  was reported [10] which was derived by several data points between  $1.4 \text{ MeV}$  and  $2.4 \text{ MeV}$ ; no extrapolation to  $S(300 \text{ keV})$  is given in [10] because of the contradicting energy dependencies of the S-factor in [4, 8]. The theoretical predictions vary between  $0.7 \text{ MeV b}$  and  $2.5 \text{ MeV b}$  at  $300 \text{ keV}$  [3, 4, 5, 6, 7, 8].

This work gives a new prediction for the direct capture cross section of the  $^{16}\text{O}(\alpha,\gamma)^{20}\text{Ne}$  reaction at low energies. The calculation is based on a systematic folding potential which is able to reproduce simultaneously scattering data for  $^{16}\text{O}(\alpha,\alpha)^{16}\text{O}$  and bound state properties of the system  $^{20}\text{Ne} = ^{16}\text{O} \otimes \alpha$  [11]. The direct capture model is presented in Sect. II. Relevant bound state properties are listed in Sect. III. The direct capture cross section is shown in Sect. IV, and the results are discussed in Sect. V. After a brief analysis of the inverse  $^{20}\text{Ne}(\gamma,\alpha)^{16}\text{O}$  photodisintegration reaction in Sect. VI, conclusions are drawn in Sect. VII.

---

\*E-mail: WidmaierMohr@compuserve.de

## II. DIRECT CAPTURE, $B(E/M\mathcal{L})$ VALUES, AND FOLDING POTENTIALS

### A. Direct Capture

The direct capture (DC) cross section for  $E1$ ,  $E2$ , and  $M1$  transitions is given in detail in Refs. [12, 13]. Here only the essential properties of the model are repeated. The DC cross section is proportional to the square of the overlap integral of the scattering wave function  $\chi_l$ , the electromagnetic transition operator  $\mathcal{O}^{E/M\mathcal{L}}$ , and the bound state wave function  $u_{NL}$ :

$$\sigma_{DC}(E) \sim \left| \int dr u_{NL}(r) \mathcal{O}^{E/M\mathcal{L}} \chi_l(r, E) \right|^2 \quad (2.1)$$

The radial parts of the dominating  $E1$ ,  $E2$ , and  $M1$  electromagnetic transition operators are given by:

$$\mathcal{O}^{E1} = \frac{3}{\rho^3} [(\rho^2 - 2) \sin \rho + 2\rho \cos \rho] r \approx r \quad (2.2)$$

$$\mathcal{O}^{E2} = \frac{15}{\rho^5} [(5\rho^2 - 12) \sin \rho + (12 - \rho^2)\rho \cos \rho] r^2 \approx r^2 \quad (2.3)$$

$$\mathcal{O}^{M1} = \frac{1}{2\rho} [\sin \rho + \rho \cos \rho] \approx 1 \quad (2.4)$$

with the so-called long wavelength approximation for  $\rho = k_\gamma r \ll 1$ . From Eq. (2.4) and from the orthogonality of the wave functions it is obvious that the  $M1$  contributions will be very small in the DC model (see Sect. IV). The exact form of the multipole operators in Eqs. (2.2), (2.3), and (2.4) was used in the following calculations.

The coefficient of proportionality in Eq. (2.1) for  $E1$  transitions contains a factor

$$\tilde{C}(E1) = [C(E1)]^2 \sim \left[ \frac{A_1 A_2}{A_1 + A_2} \left( \frac{Z_1}{A_1} - \frac{Z_2}{A_2} \right) \right]^2 \quad (2.5)$$

which describes the isospin suppression of  $E1$  transitions in  $N = Z$  nuclei between  $T = 0$  states. If one uses integer mass numbers, the  $E1$  cross section exactly vanishes; using precise masses, one calculates very small  $E1$  cross sections. In reality, small  $T = 1$  isospin admixtures in the scattering and bound state wave functions may lead to a significant enhancement of the capture cross section compared to the DC model calculation [5].

### B. $B(E/M\mathcal{L})$ values

Whereas Eq. (2.1) determines the overlap integral at an arbitrary energy  $E$  of the scattering wave function, the following Eq. (2.6) gives a similar overlap integral between bound state wave functions at their defined energies  $E_{x,i}$  and  $E_{x,f}$  for transitions  $L_i \rightarrow L_f$  [14, 15]:

$$B(E\mathcal{L}, L_i \rightarrow L_f) = \frac{e^2 \beta_{\mathcal{L}}^2 (2L_f + 1)(2\mathcal{L} + 1)}{4\pi(2L_i + 1)} \cdot \langle L_f 0 \mathcal{L} 0 | L_i 0 \rangle^2 \times \left[ \int_0^\infty u_{N_f L_f}(r) r^{\mathcal{L}} u_{N_i L_i}(r) dr \right]^2 \quad (2.6)$$

with

$$\beta_{\mathcal{L}} = \frac{A_2^{\mathcal{L}} Z_1 + (-1)^{\mathcal{L}} A_1^{\mathcal{L}} Z_2}{(A_1 + A_2)^{\mathcal{L}}} \quad (2.7)$$

The above formalism is also valid for quasi-bound states with  $E > 0$  which appear as resonances in the capture reaction.

Obviously, one finds the same suppression of  $E1$  transitions between  $T = 0$  states in  $N = Z$  nuclei because the suppression factors in Eq. (2.5) and (2.7) are identical:  $C(E1) = \beta_1$ . This identity gives the chance to renormalize the DC calculation by the ratio of experimental and calculated  $B(E\mathcal{L})$  values

$$r_{BE} = \frac{B_{\text{exp}}(E\mathcal{L})}{B_{\text{calc}}(E\mathcal{L})} \quad (2.8)$$

leading to a theoretically predicted capture cross section  $\sigma_{\text{th}}$ :

$$\sigma_{\text{th}}(E) = r_{BE} \times \sigma_{DC}(E) \quad (2.9)$$

One expects ratios  $r_{BE} \approx 1$  for  $E2$  transitions and  $r_{BE} \gg 1$  for  $E1$  transitions. Because  $M1$  transitions play only a very minor role (see Sect. IV),  $r_{BM} = 1$  was used in all cases. The expectations for the  $r_{BE}$  values are confirmed by the calculations in Sect. III.

### C. Folding Potentials

The essential ingredients for the calculation of the capture cross section and the  $B(E\mathcal{L})$  values are the potentials which are required for the calculation of the wave functions in Eqs. (2.1) and (2.6). Based on the double-folding approach, a potential has been derived in [11] which is capable of describing simultaneously elastic  $^{16}\text{O}(\alpha, \alpha)^{16}\text{O}$  scattering at energies above and below the Coulomb barrier and bound state properties of the system  $^{20}\text{Ne} = ^{16}\text{O} \otimes \alpha$ .

The potential  $V(r)$  is given by

$$V(r) = V_C(r) + \lambda V_F(r) \quad (2.10)$$

with the Coulomb potential  $V_C(r)$  of a homogeneously charged sphere with radius  $R_C$  and the folding potential  $V_F(r)$  which is scaled by a strength parameter  $\lambda$  of the order of  $\lambda \approx 1.2 - 1.3$ .

$$V_F(r) = \int \int \rho_1(r_1) \rho_2(r_2) v_{\text{eff}}(E) d^3r_1 d^3r_2 \quad (2.11)$$

$\rho_{1,2}$  are the densities of the  $\alpha$  particle and  $^{16}\text{O}$  which are derived from electron scattering data [16], and  $v_{\text{eff}}$  is an effective interaction [11, 17]. The Coulomb radius  $R_C$  has been chosen identical to the root-mean-square radius of the folding potential ( $r_{\text{rms}} = 3.603 \text{ fm}$ ).

### III. BOUND AND QUASI-BOUND STATE PROPERTIES OF $^{20}\text{Ne} = ^{16}\text{O} \otimes \alpha$

The wave function  $u_{NL}(r)$  which describes the relative motion of the  $\alpha$ -nucleus system is characterized by the node number  $N$  and the orbital angular momentum  $L$ . These values are related to the corresponding quantum numbers  $n_i$  and  $l_i$  of the four nucleons forming the  $\alpha$  cluster in the  $sd$ -shell:

$$Q = 2N + L = \sum_{i=1}^4 (2n_i + l_i) = \sum_{i=1}^4 q_i \quad (3.1)$$

One expects  $Q = 8$  for the ground state band and  $Q = 9$  for the first negative parity band. The following procedure has been used for the calculation of the wave functions and their properties. First, the strength parameter  $\lambda$  of the folding potential was adjusted to reproduce the energy of the state under consideration. Second, for resonances (which are quasi-bound states with  $E > 0$ ) the theoretical width  $\Gamma_\alpha^{\text{th}}$  was derived from scattering phase shifts  $\delta_L$  by

$$\Gamma_\alpha^{\text{th}} = \frac{2}{(d\delta_L/dE)|_{E=E_{\text{res}}, \delta_L=\pi/2}} \quad (3.2)$$

The results are listed in Table I.

One finds that the strength parameter  $\lambda$  is constant within about  $\pm 2\%$  for the ground state band with positive parity and within  $\pm 5\%$  for the negative parity band (or  $\pm 2\%$  if one neglects the  $9^-$  state with its tentative assignment to this band). The average values  $\lambda_{\text{even}}$  for the positive parity band are slightly smaller than the average  $\lambda_{\text{odd}}$  for the negative parity band. Additionally, a remarkable agreement is found between the calculated widths  $\Gamma_\alpha^{\text{th}}$  and the experimental widths  $\Gamma_\alpha^{\text{exp}}$  especially for the negative parity band; for the ground state band one finds an overestimation of the order of a factor of 6.6 (14.5) for the  $6^+$  ( $8^+$ ) state.

It is interesting to note that the potential for the  $L = 0$  partial wave roughly reproduces also the properties of the  $0_4^+$  state in  $^{20}\text{Ne}$  at  $E_x \approx 8700 \text{ keV}$ . Using exactly the same potential as for the ground state ( $\lambda = 1.2413$ ) one obtains a broad resonance with  $Q = 10$  at  $E_x^{\text{th}} \approx 8080 \text{ keV}$  with a width of several MeV. This compares well with the experimental values of the excitation energy of  $E_x^{\text{exp}} \approx 8700 \text{ keV}$  and of the experimental width  $\Gamma_\alpha^{\text{exp}} > 800 \text{ keV}$ . However, it is difficult to define the excitation energy of this broad resonance from the potential model calculation because the calculated phase shift does not reach  $\delta_0 = \pi/2$ . Instead of Eq. (3.2) a revised definition for broad resonances was used here:

$$\Gamma_\alpha^{\text{th}} = \frac{2}{(d\delta_L/dE)|_{E=E_{\text{res}}, (d\delta_L/dE)=\text{max.}}} \quad (3.3)$$

TABLE I: Properties of the  $Q = 8$  and  $Q = 9$  states in  $^{20}\text{Ne}$ . Experimental values have been taken from [18]. There is no clear assignment of  $7^-$  and  $9^-$  states to the  $0^-$  band in [18]; the lowest tentative assignment was used. Minor numerical differences to Ref. [11] are a consequence of a different Coulomb radius  $R_C$ .

$E_x$ (keV)	$E$ (keV)	$J^\pi$	$Q$	$N$	$L$	$\lambda$	$\Gamma_\alpha^{\text{exp}}$ (keV)	$\Gamma_\alpha^{\text{th}}$ (keV)
0	-4730	$0^+$	8	4	0	1.2413	—	—
1634	-3096	$2^+$	8	3	2	1.2239	—	—
4248	-482	$4^+$	8	2	4	1.2176	—	—
8778	+4048	$6^+$	8	1	6	1.1996	$0.11 \pm 0.02$	0.73
11951	+7221	$8^+$	8	0	8	1.2622	$35 \pm 10 \text{ eV}$	508 eV
5788	+1058	$1^-$	9	4	1	1.2663	$28 \pm 3 \text{ eV}$	40 eV
7156	+2426	$3^-$	9	3	3	1.2774	$8.2 \pm 0.3$	11.9
10262	+5532	$5^-$	9	2	5	1.2745	$145 \pm 40$	186
13692	+8962	$7^-$	9	1	7	1.3251	$158 \pm 18^a$	147
17430	+12700	$9^-$	9	0	9	1.4138	$52.8 \pm 7.0^b$	23.6

<sup>a</sup>derived from  $\Gamma_\alpha = 310 \pm 30 \text{ keV}$  and  $\Gamma_{\alpha_0}/\Gamma_\alpha = 0.51 \pm 0.03$

<sup>b</sup>derived from  $\Gamma_\alpha = 220 \pm 25 \text{ keV}$  and  $\Gamma_{\alpha_0}/\Gamma_\alpha = 0.24 \pm 0.01$

TABLE II:  $B(E\mathcal{L})$  values for electromagnetic transitions in  $^{20}\text{Ne}$ . Experimental values have been taken from [18].

$J_i^\pi$	$E_{x,i}$ (keV)	$J_f^\pi$	$E_{x,f}$ (keV)	$\mathcal{L}$	$B_{\text{exp}}(E\mathcal{L})$ (W.u.)	$B_{\text{th}}(E\mathcal{L})$ (W.u.)	$r_{BE}$
$2^+$	1634	$0^+$	0	2	20.3(13)	15.6	1.30
$4^+$	4248	$2^+$	1634	2	21.9(22)	21.0	1.05
$6^+$	8778	$4^+$	4248	2	19.7(30)	19.7	1.00
$8^+$	11951	$6^+$	8778	2	9.0(13)	9.5	0.95
$3^-$	7156	$1^-$	5788	2	50.1(78)	41.6	1.20
$1^-$	5788	$0^+$	0	1	$8.3(31) \times 10^{-6}$	$3.9 \times 10^{-6}$	2.13
$1^-$	5788	$2^+$	1634	1	$1.1(2) \times 10^{-4}$	$7.3 \times 10^{-6}$	15.0
$3^-$	7156	$2^+$	1634	1	—	$5.6 \times 10^{-6}$	2.13 <sup>a</sup>
$3^-$	7156	$4^+$	4248	1	$7.9(9) \times 10^{-5}$	$5.4 \times 10^{-6}$	14.7
$5^-$	10262	$4^+$	4248	1	—	$6.0 \times 10^{-6}$	2.13 <sup>a</sup>

<sup>a</sup> $r_{BE}$  assumed as for  $1^- \rightarrow 0^+$ ; no significant relevance for the  $^{16}\text{O}(\alpha, \gamma)^{20}\text{Ne}$  cross section, see Fig. 1.

In the same way, the properties of the broad  $2^+$  state in the  $0_4^+$  band are reproduced: using  $\lambda = 1.2239$ , one finds  $E_x^{\text{th}} = 9130 \text{ keV}$  and  $\Gamma_\alpha^{\text{th}} \approx 5 \text{ MeV}$  which compares to the experimental values  $E_x^{\text{exp}} = 9000 \text{ keV}$  and  $\Gamma_\alpha^{\text{exp}} \approx 800 \text{ keV}$ .

Using the potential strength parameters  $\lambda$  as given in Table I, one may calculate  $B(E\mathcal{L})$  values using Eq. (2.6) and the formalism in Sect. II B without free parameters. The results are listed in Table II which includes also the ratio  $r_{BE}$  between the experimental and theoretical values as defined in Eq. (2.8).

The above simple two-body model reproduces the partial widths  $\Gamma_\alpha$  of the states under consideration with reasonable accuracy (see Table I), and the calculated reduced transition strengths for  $E2$  transitions are in good agreement with the experimental values (see Table II). A prerequisite for the successful application of a simple two-body model is that the relevant states in  $^{20}\text{Ne}$  have a dominating  $^{16}\text{O} \otimes \alpha$  cluster structure. Such a structure can be expected from the double shell closure at  $^{16}\text{O}$ , and it is confirmed by large spectroscopic factors close to unity which have been extracted from the analysis of transfer reactions. However, it is difficult to specify precise values for the spectroscopic factors as can be seen from the results given in compilations [18, 19, 20, 21] and from recent experiments (see e.g. [22, 23, 24, 25, 26]).

## IV. RESULTS

### A. The astrophysical S-factor

The calculation of the capture cross section of the  $^{16}\text{O}(\alpha,\gamma)^{20}\text{Ne}$  capture reaction is now straightforward. The folding potentials (see Sect. II C) have been adjusted in strength to reproduce the bound state energies (see Sect. III). Consequently, the wave functions of the DC model (see Sect. II A) are well-defined. The absolute value of the capture cross section is adjusted using the ratios between the experimental and calculated  $B(E\mathcal{L})$  values (see Eq. (2.8) and Sect. II B). The results are shown in Figs. 1, 2, and 3.

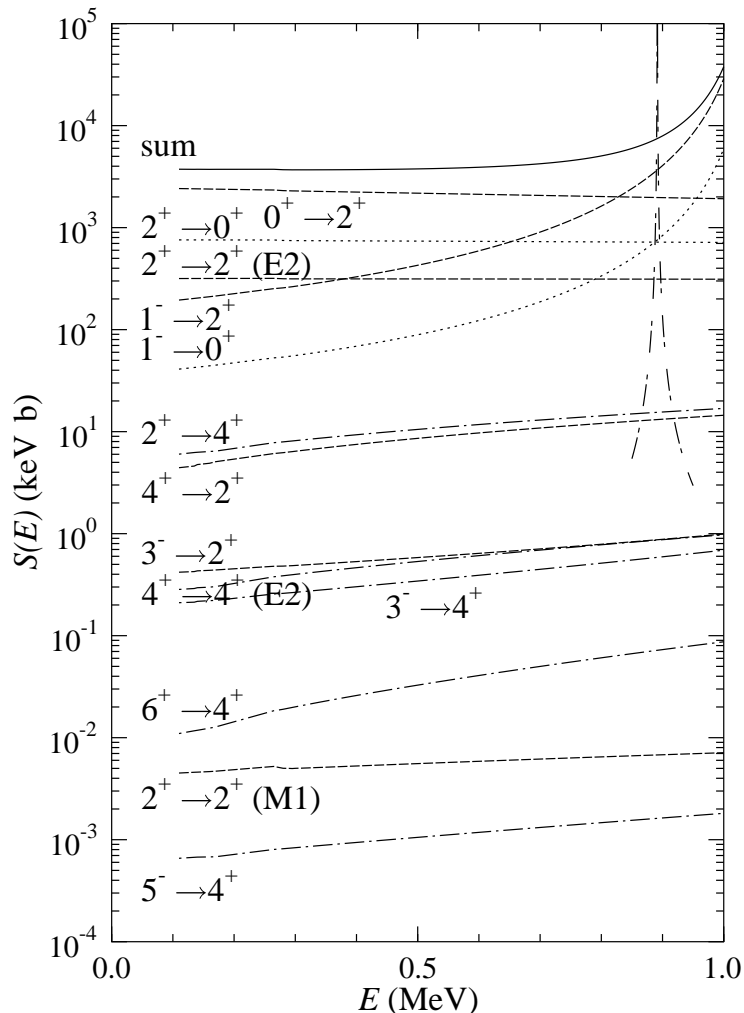


FIG. 1: S-factor of the DC cross section of the  $^{16}\text{O}(\alpha,\gamma)^{20}\text{Ne}$  capture reaction. The sum of all transitions is shown as full line. Transitions to the  $0^+$  ground state ( $2^+$  first excited state;  $4^+$  second excited state) in  $^{20}\text{Ne}$  are shown as dotted (dashed; dash-dotted) lines. The  $M1$  transition from the incoming  $L = 4$  partial wave to the  $J^\pi = 4^+$  bound state has a S-factor of less than  $6 \times 10^{-6}$  keV b (off scale). The S-factor of the narrow  $3^-$  resonance at  $E = 891$  keV has been calculated using the Breit-Wigner formula (dashed line); this resonance is not included in the model space, see Sect. V.

Fig. 1 summarizes the calculations. All possible  $E1$ ,  $E2$ , and  $M1$  transitions from the incoming partial waves with  $0 \leq L \leq 6$  to the three bound states with  $J^\pi = 0^+$ ,  $2^+$ , and  $4^+$  have been taken into account. Below  $E = 500$  keV, about two third of the total cross section comes from the incoming  $L = 0$  partial wave to the first excited  $2^+$  state. Further significant contributions from the incoming  $L = 2$  partial wave to the ground state and to the first excited state are of the order of about 20% and 10%. The DC cross section below  $E = 500$  keV is almost entirely given by  $E2$  transitions.

At energies above  $E = 500$  keV the tail of the  $1^-$  resonance at  $E = 1058$  keV becomes more and more important. Although the width of this resonance is slightly overestimated by the potential model calculation (see Table I), the

adjustment of the  $B(E\mathcal{L})$  values according to Eq. (2.8) assures that the calculated resonance strength is in agreement with the experimental value.

Transitions from partial waves with angular momentum  $L > 2$  are practically not relevant for the  $^{16}\text{O}(\alpha, \gamma)^{20}\text{Ne}$  cross section below 1 MeV. These transitions are suppressed because of the centrifugal barrier and because of the reduced transition energy for all transitions to the second excited state with  $J^\pi = 4^+$  at  $E_x = 4248$  keV. The tail of the  $3^-$  resonance at  $E = 2426$  keV is not visible at energies below  $E = 1$  MeV.

The branching ratios to the ground states with  $J^\pi = 0^+$  and the first (second) excited state with  $J^\pi = 2^+$  ( $4^+$ ) at  $E_x = 1634$  keV (4248 keV) are shown in Fig. 2. The branching ratios are almost independent of energy below  $E = 800$  keV with a strong 78 % contribution to the  $2^+$  state and a 22 % contribution to the  $0^+$  ground state. The contribution of the second excited  $4^+$  state remains below 1 % in the whole energy range under consideration.

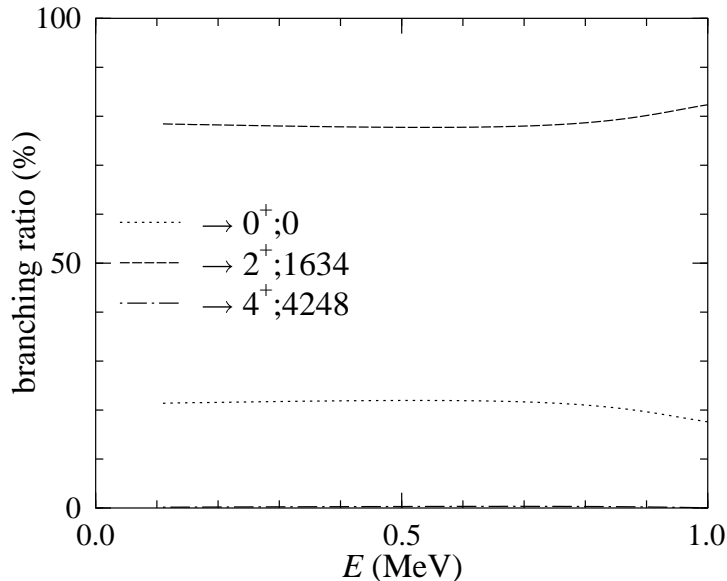


FIG. 2: Branching ratios of the DC cross section of the  $^{16}\text{O}(\alpha, \gamma)^{20}\text{Ne}$  capture reaction leading to the  $0^+$  ground state (dotted line),  $2^+$  state at  $E_x = 1634$  keV (dashed line), and  $4^+$  state at  $E_x = 4248$  keV (dash-dotted line; below 1%, practically not visible).

Experimentally upper limits have been determined for the S-factor to the  $0^+$  ground state ( $S \rightarrow 0^+ < 920$  keV b) and to the  $2^+$  state ( $S \rightarrow 2^+ < 2450$  keV b) [10] from measurements between resonances at higher energies. The predictions from the DC model calculation are  $S \rightarrow 0^+ = 802$  keV b and  $S \rightarrow 2^+ = 2877$  keV b at  $E = 300$  keV. Because of the energy dependence of the S-factor, the calculated values do not contradict the experimental limits of [10]. In a similar way as in [10] a total S-factor of  $S(300 \text{ keV}) = 700 \pm 300$  keV b is derived in [9]. However, the result of [9] has been questioned by [4]: the experimental data of [9] at energies around 2 MeV were extrapolated to 300 keV using the probably unrealistic energy dependence of the S-factor from [8] (see discussion in [4, 6]); it is stated that this result “should at least be multiplied by a factor of two” [4]. Additionally, the upper limit of [9] was derived close to the  $0^+$  resonance at 1991 keV; consequently the derived upper limit depends sensitively on the chosen resonance parameters (strength and width) of this resonance [10].

An estimate of the theoretical uncertainties can be done in the following way. Obviously, the calculated cross sections, which have been adjusted to experimental  $B(E\mathcal{L})$  values according to Eq. (2.8), depend on the experimental  $B(E\mathcal{L})$  values or  $\Gamma_\gamma$  partial widths. Because  $\Gamma_\alpha \gg \Gamma_\gamma$  for all resonances under consideration, the radiation width  $\Gamma_\gamma$  may also be obtained from the resonance strength  $\omega\gamma$  of a resonance in the  $^{16}\text{O}(\alpha, \gamma)^{20}\text{Ne}$  capture reaction. Typical experimental uncertainties for the resonance strengths are of the order of about 15 % [1], and results from different experiments also agree with each other at the 15 % level. Combining these uncertainties, this leads to a total uncertainty of about 20 % for the experimental  $B(E\mathcal{L})$  values or radiation widths  $\Gamma_\gamma$ . A second source of uncertainties comes from the adjustment of the potential strength to the binding energies of (quasi-)bound states (see Table I). The numerical adjustment itself can be done with negligible uncertainties; however, the model assumes a pure two-body configuration for all states, and consequently, the adjustment of the potential may be somewhat uncertain. But it has been shown in [11], that the potential reproduces experimental phase shifts with reasonable quality. Additionally, almost the same potential strength parameter  $\lambda$  has been found for all states with positive parity; an uncertainty of about 2 % can be seen from Table I. The dependence of the S-factor or capture cross section on the potential strength

was calculated using a variation of the parameter  $\lambda$  of  $\pm 2\%$ . For the dominating transition from the incoming  $L = 0$  partial wave to the  $2^+$  bound state one obtains a variation of the S-factor of  $+14\%$  ( $-15\%$ ) for a  $2\%$  enhanced (reduced) potential strength. Combining all the above uncertainties, a careful estimate of the total uncertainty of the S-factor is about  $30\%$ .

### B. The astrophysical reaction rate $N_A \langle \sigma v \rangle$

For the calculation of the astrophysical reaction rate  $N_A \langle \sigma v \rangle$  in the temperature range where DC is dominating, one needs the S-factor from very low energies to about  $500 \text{ keV}$ . A second-order polynomial has been fitted to the calculated S-factor which is shown in Fig. 3 in linear scale:

$$S(E) = 3808 \text{ keV b} - 864 \text{ keV b} \times E/\text{MeV} + 1527 \text{ keV b} \times (E/\text{MeV})^2 \quad (4.1)$$

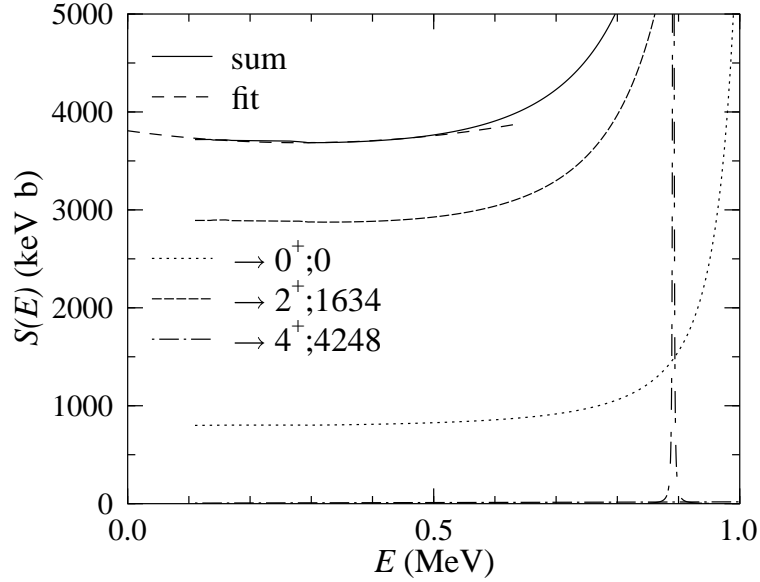


FIG. 3: S-factor of the  $^{16}\text{O}(\alpha, \gamma)^{20}\text{Ne}$  reaction in linear scale (same as Fig. 1). For extrapolation to  $E \rightarrow 0$ , the S-factor has been fitted using a second-order polynomial  $S(E) = 3808 \text{ keV b} - 864 \text{ keV b} \times E/\text{MeV} + 1527 \text{ keV b} \times (E/\text{MeV})^2$  up to  $E = 0.5 \text{ MeV}$  (long-dashed line). The S-factor of the narrow  $3^-$  resonance at  $E = 891 \text{ keV}$  has been calculated using the Breit-Wigner formula (dashed line); this resonance is not included in the model space, see Sect. V.

Because of the weak energy dependence of the S-factor the reaction rate can be calculated using the approximation

$$N_A \langle \sigma v \rangle = N_A \left( \frac{2}{\mu} \right)^{1/2} \frac{\Delta}{(kT)^{3/2}} S(E_0) \left( 1 + \frac{5}{12\tau} \right) \exp(-\tau) \quad (4.2)$$

with  $E_0$  and  $\Delta$  as defined in Sect. I and  $\tau = 3E_0/(kT)$ . Compared to [1], a somewhat larger reaction rate is obtained because of the larger S-factor at the relevant energies (see Fig. 4).

At temperatures below  $T_9 \approx 0.2$  the reaction rate is almost entirely given by the DC contribution. Because of the increased S-factor at low energies, the reaction rate is enhanced by the same factor. The almost constant ratio below  $T_9 = 0.2$  in Fig. 4 arises from the fact that the energy dependence of the S-factor is practically the same in this work and in [1] which was adopted from [3] (see also Sect. V). At higher energies the reaction rate is dominated by the resonant contributions, and hence the increased DC cross section has no significant influence on the reaction rate.

No distinction is made here between the reaction rates  $N_A \langle \sigma v \rangle^*$  under stellar conditions and  $N_A \langle \sigma v \rangle_{\text{lab}}$  in the laboratory. Both rates are practically identical up to temperatures of about  $T_9 = 3$  [1]. There is not significant thermal population of excited states in  $^{16}\text{O}$  which are located at excitation energies above  $E_x = 6 \text{ MeV}$ . The stellar reaction rate  $N_A \langle \sigma v \rangle^*$  can directly be derived from experimental data.

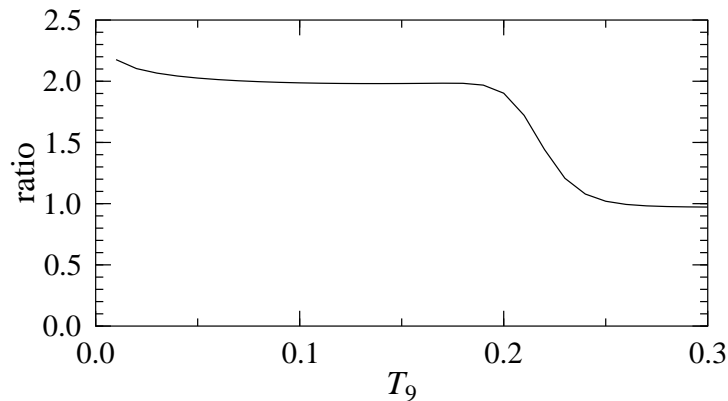


FIG. 4: Ratio between the reaction rate  $N_A \langle \sigma v \rangle$  calculated from the DC model and folding potentials (this work) and the NACRE compilation [1]. Because of the increased DC cross section at low energies, the reaction rate is about a factor of two larger than the NACRE rate below  $T_9 = 0.2$  where DC is dominating.

## V. DISCUSSION

Because of the properties of the doubly-magic  $^4\text{He}$  and  $^{16}\text{O}$  nuclei a simple two-body model should be able to describe scattering phase shifts, bound state properties of  $^{20}\text{Ne}$ , and the capture cross section of the  $^{16}\text{O}(\alpha, \gamma)^{20}\text{Ne}$  reaction with reasonable accuracy [6, 7, 8]. The combination of the model with systematic folding potentials ensures a good description of elastic scattering cross sections and phase shifts at low energies.

The strength parameter  $\lambda$  is adjusted to the binding energies of low-lying states in  $^{20}\text{Ne}$ ; this guarantees the correct asymptotic behavior of the bound state wave functions at large distances which is important for the calculation of the  $^{16}\text{O}(\alpha, \gamma)^{20}\text{Ne}$  capture cross section. The correct behavior of the wave functions at small distances, i.e. the number of nodes of the wave function and their positions, is obtained from Eq. (3.1) which avoids Pauli-forbidden states. The precise influence of antisymmetrization of the 20-nucleon wave function has been discussed in detail in [6]; it has been pointed out “the smallness of the residual antisymmetrization terms” because of the shell closures in  $^4\text{He}$  and  $^{16}\text{O}$ .

The potential in the chosen model automatically contains eigenstates at energies below and above the  $^{16}\text{O}-\alpha$  threshold. The quasi-bound states above the threshold appear as resonances in the  $^{16}\text{O}(\alpha, \alpha)^{16}\text{O}$  scattering phase shifts and in the  $^{16}\text{O}(\alpha, \gamma)^{20}\text{Ne}$  capture cross section. As already pointed out in [6], the term “direct capture” may be misleading in this case. Further details on such so-called potential resonances are given in [27, 28, 29]. However, the model contains only a limited number of eigenstates. It is not possible to include all resonances of the  $^{16}\text{O}(\alpha, \gamma)^{20}\text{Ne}$  reaction in this simple two-body model. E.g., the states with dominating  $^{16}\text{O}(3^-) \otimes \alpha$  structure at  $E_x = 4967$  keV ( $E = 237$  keV; no resonance because of the unnatural  $2^-$  parity) and 5621 keV ( $E = 891$  keV) are not included in the model; the inclusion of such states requires e.g. a multicluster model [3]. The influence of the  $3^-$  resonance at 891 keV at low energies is negligible as can be seen from Figs. 1 and 3. The S-factor of this resonance has been calculated from the Breit-Wigner formula using the known widths and strength [1, 18].

The calculation of the overlap integrals in Eq. (2.1) depends sensitively on the shape of the wave functions especially for wave functions with several nodes. Minor shifts of the nodes may reduce or enhance the overlap integral significantly because of cancellation effects between positive and negative regions of the integrand in Eq. (2.1) (see Figs. 2-5 of Ref. [6]). This leads to a relatively sensitive dependence of the  $^{16}\text{O}(\alpha, \gamma)^{20}\text{Ne}$  cross section on the chosen potential, i.e. the potential strength parameter  $\lambda$ . A variation of  $\lambda$  by its uncertainty of  $\pm 2\%$  (see Table I) changes the capture cross section already by about 15% which has to be considered as the intrinsic model uncertainty. Further uncertainties as discussed in Sect. IV A lead to a total uncertainty of the calculated S-factor of about 30%.

The adjustment of the DC cross sections of the  $^{16}\text{O}(\alpha, \gamma)^{20}\text{Ne}$  reaction using the ratios between experimental and theoretical  $B(E\mathcal{L})$  according to Eq. (2.8) gives the chance to include E1 transitions in the DC model. As stated earlier (see Eqs. (2.5), (2.7), and Sect. II), E1 transitions are suppressed in the DC model. A detailed microscopic investigation of E1 transitions in the  $^{16}\text{O}(\alpha, \gamma)^{20}\text{Ne}$  reaction was able to reproduce the approximate strength of the transitions, but showed problems with the branching ratios [5]. Therefore the usage of Eq. (2.8) seems to be the best way to predict the E1 part of the  $^{16}\text{O}(\alpha, \gamma)^{20}\text{Ne}$  cross section at low energies: the energy dependence of the cross section is provided by the model, and the absolute strength and the branching ratio are obtained from the adjustment to experimental data. The total contribution of E1 transitions to the  $^{16}\text{O}(\alpha, \gamma)^{20}\text{Ne}$  cross section remains small as long as energies significantly below the  $1^-$  resonance at 1058 keV are considered.

The final result for the total S-factor at 300 keV is  $S(300 \text{ keV}) = 3.7 \pm 1.2 \text{ MeV b}$  which is slightly higher than



previous calculations [3, 4, 5, 6, 7, 8] but overlaps with the range of the results of [3, 4, 5, 6, 7] within the estimated uncertainties. The result of [8] is significantly lower but has been questioned in [6]. The calculated slope  $a$  of the S-factor at low energies, usually defined as

$$a = \frac{1}{S(0)} \left( \frac{dS}{dE} \right)_{E=0} \quad (5.1)$$

is in good agreement with previous calculations:  $a = -0.23 \text{ MeV}^{-1}$  from this work for the total S-factor is almost identical to  $a = -0.21 \text{ MeV}^{-1}$  for the dominating  $L = 0 \rightarrow 2^+$  transition in [6]. The S-factor decreases slightly with increasing energy in all calculations [3, 4, 5, 6, 7]. The only exception is the result of [8] who finds an increasing S-factor with increasing energy with values of  $a \approx +0.6 \text{ MeV}^{-1}$ . A possible shortcoming of [8] is discussed in [6].

Branching ratios  $b$ , here often defined as

$$b = \frac{S_0 + S_2}{S_0} \quad (5.2)$$

can be estimated from Fig. 5 of [3] to be of the order of  $3 \lesssim b \lesssim 3.5$ , and  $b \approx 4.3$  is given in [4]. In this work  $b = 4.5$  is found. Again this calculation agrees nicely with the microscopic calculations by [3, 4].

Any comparison with experimental data is difficult. No experimental data are available at energies below 1 MeV, and the extraction of the DC contribution from experimental data at higher energies is hampered by the dominating resonant contributions. As pointed out in [10], the extraction of the DC cross section depends sensitively on the chosen resonance parameters, because the DC cross section is usually determined as the difference between the measured cross section and the calculated resonant cross section in the tail of a resonance with Breit-Wigner shape. As pointed out already in Sect. IV A, the new calculation does not contradict the upper limits of [10].

Finally, the astrophysical reaction rate  $N_A \langle \sigma v \rangle$  is about a factor of two higher than in the NACRE compilation [1] below  $T_9 = 0.2$  because the S-factor at low energies is about  $3.7 \text{ MeV b}$  in this work compared to the adopted value of  $2 \text{ MeV b}$  in [1]. A detailed analysis of the astrophysical consequences is beyond the scope of this paper; in general, the  $^{16}\text{O}(\alpha, \gamma)^{20}\text{Ne}$  reaction rate is still low enough to block the reaction chain  $3\alpha \rightarrow ^{12}\text{C}(\alpha, \gamma)^{16}\text{O}(\alpha, \gamma)^{20}\text{Ne}$ . Using the NACRE rate for the  $^{12}\text{C}(\alpha, \gamma)^{16}\text{O}$  reaction and the new rate for the  $^{16}\text{O}(\alpha, \gamma)^{20}\text{Ne}$  reaction, one finds at  $T_9 = 0.2$  a ratio of about  $5 \times 10^{-5}$  between the  $^{16}\text{O}(\alpha, \gamma)^{20}\text{Ne}$  and the  $^{12}\text{C}(\alpha, \gamma)^{16}\text{O}$  rates. For comparison, abundances calculated from the NACRE rates can be found in [30].

## VI. THE INVERSE $^{20}\text{Ne}(\gamma, \alpha)^{16}\text{O}$ REACTION

Reverse reaction rates  $\lambda^*$  under stellar conditions are usually derived from the detailed balance theorem [1, 31] which reads for the case of the  $^{16}\text{O}(\alpha, \gamma)^{20}\text{Ne}$  and  $^{20}\text{Ne}(\gamma, \alpha)^{16}\text{O}$  reactions

$$\frac{\lambda^*}{\langle \sigma v \rangle} = \left( \frac{\mu kT}{2\pi\hbar^2} \right)^{3/2} \exp \left( -\frac{Q}{kT} \right) \quad (6.1)$$

because the partition functions do not deviate significantly from unity for the nuclei  $^4\text{He}$ ,  $^{16}\text{O}$ , and  $^{20}\text{Ne}$  up to temperatures of  $T_9 \approx 3$  [1] because of the large excitation energies of the first excited states ( $^{16}\text{O}$ :  $E_x = 6049 \text{ keV}$ ,  $0^+$ ;  $^{20}\text{Ne}$ :  $E_x = 1634 \text{ keV}$ ,  $2^+$ ). The reaction  $Q$ -value is  $Q = +4730 \text{ keV}$ . It has been shown in [32] that the detailed balance theorem remains valid for resonant transitions although the thermal occupation probability is extremely small for the first excited state in  $^{20}\text{Ne}$  and negligible for  $^{16}\text{O}$  for all astrophysically relevant temperatures.

The same arguments as given in [32] hold for the non-resonant case at temperatures below  $T_9 = 0.2$  (although the photodisintegration rate is practically negligible at such low temperatures). The reaction rate  $\lambda_i$  of the  $^{20}\text{Ne}(\gamma, \alpha)^{16}\text{O}$  photodisintegration reaction for a given state  $i$  in  $^{20}\text{Ne}$  is given by

$$\begin{aligned} \lambda_i &= c \int_{Q-E_{x,i}}^{\infty} n_{\gamma}(E_{\gamma}, T) \sigma_i^{(\gamma, \alpha)}(E_{\gamma}) dE_{\gamma} \\ &\approx \frac{c}{\pi^2} \frac{1}{(\hbar c)^3} \frac{\mu c^2}{(2I_i + 1)} \exp \left( \frac{+E_{x,i} - Q}{kT} \right) \int_0^{\infty} \exp \left( -\frac{E_{\alpha}}{kT} - 2\pi\eta \right) S_i(E_{\alpha}) dE_{\alpha} \end{aligned} \quad (6.2)$$

with the thermal photon density

$$n_{\gamma}(E_{\gamma}, T) dE_{\gamma} = \frac{1}{\pi^2} \frac{1}{(\hbar c)^3} \frac{E_{\gamma}^2}{\exp(E_{\gamma}/kT) - 1} dE_{\gamma} \quad (6.3)$$

(see e.g. [33]), the excitation energy  $E_{x,i}$  and the spin  $I_i$  of the  $i$ -th state, the Sommerfeld parameter  $\eta$ , and the astrophysical S-factor  $S_i$  for the transition to the  $i$ -th state in  $^{20}\text{Ne}$ . The derivation of Eq. (6.2) uses only the time reversal symmetry for the cross sections of transitions between individual states [31, 34]. Note that the energies are related by

$$E_\gamma = Q + E_\alpha - E_{x,i} \quad (6.4)$$

with  $E_\alpha$  in the center-of-mass system. This means that the required photon energy  $E_\gamma$  for the photodisintegration of  $^{20}\text{Ne}$  is reduced by the excitation energy  $E_{x,i}$  of the  $i$ -th state in  $^{20}\text{Ne}$ . Consequently, the reaction rate  $\lambda_i$  of the  $i$ -th state is enhanced by a factor  $\exp\left(+\frac{E_{x,i}}{kT}\right)$  because of the enhanced photon density at lower photon energies.

After summing all the rates according to Eq. (6.2) with their proper thermal weights proportional to the Boltzmann factor  $\exp\left(-\frac{E_{x,i}}{kT}\right)$  under stellar conditions one obtains a stellar reaction rate

$$\lambda^* \approx \frac{c}{\pi^2} \frac{1}{(\hbar c)^3} \mu c^2 \exp\left(-\frac{Q}{kT}\right) \int_0^\infty \exp\left(-\frac{E_\alpha}{kT} - 2\pi\eta\right) S_{\text{tot}}(E_\alpha) dE_\alpha \quad (6.5)$$

with the total astrophysical S-factor  $S_{\text{tot}} = \sum_i S_i$  for the  $^{16}\text{O}(\alpha, \gamma)^{20}\text{Ne}$  capture reaction. The comparison of Eq. (6.5) with the usual definition of the reaction rate of the capture reaction leads directly to the detailed balance result in Eq. (6.1). By the way, the analysis of the integrand in Eq. (6.5) together with Eq. (6.4) shows that the most effective energy for the inverse photodisintegration reaction is located at  $E_x(^{20}\text{Ne}) = Q + E_0$  where  $E_0$  is the most effective energy of the capture reaction as defined in Sect. I. Further details on the Gamow window for  $(\gamma, \alpha)$  reactions see [35].

Although their thermal occupation probabilities are extremely low because of the Boltzmann factor, excited states play a significant role in the photodisintegration process because the Boltzmann factor is exactly balanced by an enhancement factor because of the lower required photon energy according to Eqs. (6.3) and (6.4). In the case of the  $^{20}\text{Ne}(\gamma, \alpha)^{16}\text{O}$  photodisintegration reaction, the first excited state in  $^{20}\text{Ne}$  contributes with 78 % to the photodisintegration rate  $\lambda^*$  because of the 78 % branching to this state in the  $^{16}\text{O}(\alpha, \gamma)^{20}\text{Ne}$  capture reaction although the thermal occupation probability e.g. at  $T_9 = 0.2$  is below  $10^{-40}$ ! But there is no significant contribution of the first excited state in  $^{16}\text{O}$  neither to the  $^{16}\text{O}(\alpha, \gamma)^{20}\text{Ne}$  capture reaction nor to the  $^{20}\text{Ne}(\gamma, \alpha)^{16}\text{O}$  photodisintegration reaction because there is no compensation in the cross section or reaction rate for the suppression factor from the Boltzmann statistics.

Experimentally, photodisintegration rates in the laboratory can be measured using quasi-thermal photon spectra [33, 36]. Contrary to the capture rate (see Sect. IV B), the photodisintegration rates  $\lambda^*$  under stellar conditions and  $\lambda_{\text{lab}}$  in the laboratory are not identical:  $\lambda^* \neq \lambda_{\text{lab}}$ ! The laboratory experiment provides  $\lambda_{\text{lab}}$  with the target  $^{20}\text{Ne}$  in its ground state which is given by Eq. (6.2) for  $i = \text{g.s.}$ ; compared to Eq. (6.5) one finds a ratio of

$$\frac{\lambda_{\text{lab}}(T)}{\lambda^*(T)} \approx \frac{S_{\text{g.s.}}(E_0)}{S_{\text{tot}}(E_0)} \approx 0.22 \quad (6.6)$$

around  $T_9 = 0.2$  for the  $^{20}\text{Ne}(\gamma, \alpha)^{16}\text{O}$  reaction.  $E_0$  is the most effective energy of the capture reaction at temperature  $T$ , see Sect. I. Provided that the branching ratio  $S_{\text{g.s.}}/S_{\text{tot}}$  is experimentally known, the stellar rate  $\lambda^*$  can easily be derived from the experimental result  $\lambda_{\text{lab}}$ . Otherwise, theoretical models have to be used to determine  $\lambda^*$  from  $\lambda_{\text{lab}}$ . In any case, experimental data may provide helpful information to restrict theoretical calculations of the laboratory cross section or rate [37]. Further information on photodisintegration experiments for the  $^{20}\text{Ne}(\gamma, \alpha)^{16}\text{O}$  reaction is given in [32].

## VII. SUMMARY AND CONCLUSIONS

The cross section of the  $^{16}\text{O}(\alpha, \gamma)^{20}\text{Ne}$  capture reaction has been calculated using a simple two-body DC model together with systematic folding potentials. The adjustment of the potential strength and the reduced transition probabilities to the relevant experimental quantities enables the calculation of all relevant E1, E2, and M1 transitions between incoming partial waves with  $0 \leq L \leq 6$  and all bound states ( $J^\pi = 0^+$ ,  $E_x = 0$ ;  $2^+$ , 1634 keV; and  $4^+$ , 4248 keV) in  $^{20}\text{Ne}$  without further free parameters.

The astrophysical S-factor at energies below 1 MeV is somewhat higher than in previous calculations [3, 4, 5, 6, 7], whereas the energy dependence and the branching ratio to the final states is in good agreement. Consequently, the astrophysical reaction rate is enhanced compared to a recent compilation [1] at temperatures below  $T_9 = 0.2$  where the direct capture contribution is dominating.

The astrophysical reaction rate of the inverse  $^{20}\text{Ne}(\gamma, \alpha)^{16}\text{O}$  photodisintegration reaction has a significant contribution of the thermally excited first excited state in  $^{20}\text{Ne}$  although the thermal occupation probability seems to be negligible. The widely used detailed balance theorem remains valid also for the case of high-lying first excited states.

## Acknowledgments

I thank C. Angulo, P. Descouvemont, Zs. Fülöp, G. Staudt, and H. Utsunomiya for encouraging discussions.

- 
- [1] C. Angulo *et al.*, Nucl. Phys. **A656**, 1 (1999).
  - [2] F.-K. Thielemann and W. D. Arnett, Astroph. J. **295**, 604 (1985).
  - [3] M. Dufour, P. Descouvemont, and D. Baye, Phys. Rev. C **50**, 795 (1994).
  - [4] D. Baye and P. Descouvemont, Phys. Rev. C **38**, 2463 (1988).
  - [5] P. Descouvemont and D. Baye, Nucl. Phys. **A459**, 374 (1986).
  - [6] D. Baye and P. Descouvemont, Ann. Phys. **165**, 115 (1985).
  - [7] P. Descouvemont and D. Baye, Phys. Lett. B **127**, 286 (1983).
  - [8] K. Langanke, Phys. Lett. B **131**, 21 (1983).
  - [9] K. H. Hahn, K. H. Chang, T. R. Donoghue, and B. W. Filippone, Phys. Rev. C **36**, 892 (1987).
  - [10] H. Knee, Ph.D. thesis, Universität Stuttgart, (Aachen: Shaker 1994).
  - [11] H. Abele and G. Staudt, Phys. Rev. C **47**, 742 (1993).
  - [12] K. H. Kim, M. H. Park, and B. T. Kim, Phys. Rev. C **35**, 363 (1987).
  - [13] P. Mohr, H. Abele, R. Zwiebel, G. Staudt, H. Krauss, H. Oberhummer, A. Denker, J. W. Hammer, and G. Wolf, Phys. Rev. C **48**, 1420 (1993).
  - [14] B. Buck and A. A. Pilt, Nucl. Phys. **A280**, 133 (1977).
  - [15] F. Hoyler, P. Mohr, and G. Staudt, Phys. Rev. C **50**, 2631 (1994).
  - [16] H. de Vries, C. W. de Jager, and C. de Vries, At. Data Nucl. Data Tables **36**, 495 (1987).
  - [17] A. M. Kobos, B. A. Brown, R. Lindsay, and R. Satchler, Nucl. Phys. **A425**, 205 (1984).
  - [18] D. R. Tilley *et al.*, Nucl. Phys. **A636**, (1998) 247, revised online version from 08 November 2000.
  - [19] F. Ajzenberg-Selove, Nucl. Phys. **A475**, 1 (1987).
  - [20] F. Ajzenberg-Selove, Nucl. Phys. **A392**, 1 (1983).
  - [21] F. Ajzenberg-Selove, Nucl. Phys. **A300**, 1 (1978).
  - [22] Z. Q. Mao, H. T. Fortune, and A. G. Lacaze, Phys. Rev. C **53**, 1197 (1996).
  - [23] T. Tanabe, M. Yasue, K. Sato, K. Ogino, Y. Kadota, Y. Taniguchi, K. Obori, K. Makino, and M. Tochi, Phys. Rev. C **24**, 2556 (1981).
  - [24] T. Tanabe, M. Yasue, K. Sato, K. Ogino, Y. Kadota, Y. Taniguchi, K. Makino and M. Tochi, Phys. Lett. B **100**, 241 (1981).
  - [25] N. Anantaraman, H. E. Gove, R. A. Lindgren, J. Töke, J. P. Trentelman, J. P. Draayer, F. C. Jundt, and G. Guillaume, Nucl. Phys. **A313**, 445 (1979).
  - [26] H. S. Bradlow, W. D. M. Rae, P. S. Fisher, N. S. Godwin, G. Proudfoot, and D. Sinclair, Nucl. Phys. **A314**, 171 (1979).
  - [27] P. Mohr, V. Kölle, S. Wilmes, U. Atzrott, G. Staudt, J. W. Hammer, H. Krauss, and H. Oberhummer, Phys. Rev. C **50**, 1543 (1994).
  - [28] P. Mohr, H. Beer, H. Oberhummer, W. Rochow, P. V. Sedyshev, S. Volz, and A. Zilges, Phys. Rev. C **60**, 017603 (1999).
  - [29] P. Mohr, Phys. Rev. C **67**, 065802 (2003).
  - [30] M. Arnould, S. Goriely, and A. Jorissen, Astron. Astroph. **347**, 572 (1999).
  - [31] W. A. Fowler, G. R. Caughlan, and B. A. Zimmerman, Ann. Rev. Astron. Astroph. **5**, 525 (1967).
  - [32] P. Mohr, C. Angulo, P. Descouvemont, and H. Utsunomiya, Proc. *Nuclear Physics in Astrophysics II*, Debrecen 2005, Ed. Zs. Fülöp *et al.*, Europ. Phys. J., in press (2005); *astro-ph/0506099*.
  - [33] P. Mohr, K. Vogt, M. Babilon, J. Enders, T. Hartmann, C. Hutter, T. Rauscher, S. Volz, and A. Zilges, Phys. Lett. B **488**, 127 (2000).
  - [34] J. M. Blatt and V. F. Weisskopf, *Theoretical Nuclear Physics*, (Wiley, New York, 1952).
  - [35] P. Mohr, M. Babilon, D. Galaviz, K. Sonnabend, K. Vogt, and A. Zilges, Nucl. Phys. **A719**, 90c (2003).
  - [36] H. Utsunomiya *et al.*, Nucl. Inst. Meth. Phys. Res. A **538**, 225 (2005).
  - [37] T. Rauscher and F.-K. Thielemann, At. Data Nucl. Data Tables **88**, 1 (2004).